# Star Formation History and Transition Epoch of Cluster Galaxies Based on the Horizon-AGN Simulation

Seyoung Jeon, Sukyoung K. Yi, Yohan Dubois, Aeree Chung, Julien Devriendt, San Han, Ryan A. Jackson, Taysun Kimm, Christophe Pichon, Jinsu Rhee

The Astrophysical Journal, 941:5 (13pp), 2022 December 10 https://doi.org/10.3847/1538-4357/ac9d8c


# Star Formation History and Transition Epoch of Cluster Galaxies Based on the Horizon-AGN Simulation

Seyoung Jeon[1], Sukyoung K. Yi[1], Yohan Dubois[2], Aeree Chung[1], Julien Devriendt[3], San Han[1], Ryan A. Jackson[1], Taysun Kimm[1], Christophe Pichon[2,4], and Jinsu Rhee[1]
[1] Department of Astronomy and Yonsei University Observatory, 50 Yonsei-ro, Seodaemun-gu, Seoul 03722, Republic of Korea; yi@yonsei.ac.kr
[2] Institut d' Astrophysique de Paris, Sorbonne Universités, et CNRS, UMP 7095, 98 bis bd Arago, 75014 Paris, France
[3] Department of Physics, University of Oxford, Keble Road, Oxford OX1 3RH, UK
[4] IPhT, DRF-INP, UMR 3680, CEA, L'Orme des Merisiers, Bt 774, 91191 Gif-sur-Yvette, France
*Received 2022 June 3; revised 2022 October 5; accepted 2022 October 24; published 2022 December 7*

## Abstract

Cluster galaxies exhibit substantially lower star formation rates than field galaxies today, but it is conceivable that clusters were sites of more active star formation in the early universe. Herein, we present an interpretation of the star formation history (SFH) of group/cluster galaxies based on the large-scale cosmological hydrodynamic simulation, Horizon-AGN. We find that massive galaxies in general have small values of *e*-folding timescales of star formation decay (i.e., "mass quenching") regardless of their environment, while low-mass galaxies exhibit prominent environmental dependence. In massive host halos (i.e., clusters), the *e*-folding timescales of low-mass galaxies are further decreased if they reside in such halos for a longer period of time. This "environmental quenching" trend is consistent with the theoretical expectation from ram pressure stripping. Furthermore, we define a "transition epoch" as where cluster galaxies become less star-forming than field galaxies. The transition epoch of group/cluster galaxies varies according to their stellar and host-cluster halo masses. Low-mass galaxies in massive clusters show the earliest transition epoch of ∼7.6 Gyr ago in lookback time. However, this decreases to ∼5.2 Gyr for massive galaxies in low-mass clusters. Based on our findings, we can describe a cluster galaxy's SFH with regard to the cluster halo-to-stellar mass ratio.

*Unified Astronomy Thesaurus concepts:* Galaxy evolution (594); Galaxy clusters (584); Galaxy quenching (2040)

## 1. Introduction

During recent decades, an enormous amount of information on galaxies has been gathered. Despite the diversity and complexity of observed galaxy properties, many interesting statistics and relationships have emerged through numerous observational surveys. Galaxies are often separated into red and blue galaxies on the color–magnitude plane, forming the red sequence and the blue cloud (e.g., Strateva et al. 2001; Baldry et al. 2004). For example, the colors and the morphology of galaxies have a robust correlation with the environment (e.g., Dressler 1980; Hogg et al. 2003). While the majority of galaxies in the universe are "live" and star-forming, most member galaxies of massive clusters are mysteriously "red and dead" with significantly depressed star formation rates (SFRs; e.g., Balogh et al. 1999; Boselli & Gavazzi 2006).

Various quenching processes have been proposed to explain the aforementioned diversities (in this study, "quenched" refers to the cessation as well as the overall decline of star formation in the long term) and these processes are classified as internal and external. Internal quenching regulates star formation mainly via feedback processes inside the galaxy. For example, energy generated by an active galactic nucleus (AGN) heats the surrounding cold gas and directly transfers momentum, inhibiting the inflow of cold gas and regulating star formation, especially in the case of massive galaxies (Croton et al. 2006; Rafferty et al. 2006; Fabian 2012; Peirani et al. 2017). In addition, stellar feedback can suppress star formation in various ways and is suggested to be the main quenching mechanism in low-mass galaxies in which gas is bound in a shallow potential well. Supernova explosions provide energy and momentum to the surrounding interstellar medium (ISM), which can disturb cold gas and prevent it from collapsing (Larson 1974; Dekel & Silk 1986; Governato et al. 2010). Moreover, ultraviolet (UV) radiation generated by young massive stars contributes to quenching of star formation through photoionization, which ionizes the surrounding cold gas and increases the gas pressure, or by direct radiative pressure (Larson & Starrfield 1971; Whitworth 1979; Hopkins et al. 2020).

Alternatively, environmental effects could affect the SFR of galaxies in dense regions, where massive dark matter halos are formed. For the galaxies orbiting in the deep gravitational potential well of a massive halo, their baryon and dark matter components are disrupted by tidal forces (i.e., tidal stripping; Richstone 1976; Gnedin 2003; Smith et al. 2016). When a galaxy moves in a cluster environment, the hot intracluster medium (ICM) can strip the ISM of the galaxy, which is the fuel for star formation (i.e., ram pressure stripping; Gunn et al. 1972; Quilis et al. 2000; Chung et al. 2007; Tonnesen et al. 2007). Otherwise, the ICM can suppress the cooling of hot gas, which consequently reduces the supply of cold gas to the galaxy (i.e., starvation or strangulation; Larson et al. 1980; Balogh et al. 2000). In dense regions, galaxies experience fly-by encounters and even mergers with nearby galaxies, resulting in the distortion of galactic structures (i.e., harassment and mergers; Moore et al. 1996, 1998; Yi et al. 2013; Smith et al. 2015; Sheen et al. 2016). Even in low-mass host halos, galaxies may already experience environmental effects before infalling into a cluster halo (i.e., preprocessing; Mihos 2004; De Lucia et al. 2012; Han et al. 2018; Jung et al. 2018).

Various quenching processes act with different timescales and magnitudes and are accumulated throughout the history of a galaxy's evolution (Iyer et al. 2020). Therefore, the star formation history (SFH) contains cumulative information about the quenching processes a galaxy has experienced. As galaxies with different internal properties and external environments may have taken distinct evolutionary paths, we can connect their physical properties and SFHs. Massive and quiescent galaxies are believed to have experienced an early phase of vigorous star formation and subsequent rapid quenching, whereas low-mass galaxies are thought to have a relatively extended SFH (e.g., Thomas et al. 2005; Ellison et al. 2018). Likewise, cluster galaxies can have different SFHs to field galaxies. Although cluster galaxies are redder and more quenched than field galaxies at the present epoch, increased fractions of blue galaxies exist in high-$z$ clusters (Butcher & Oemler 1978; Alberts et al. 2013). For example, it has been found that at $z \sim 1$ cluster galaxies have comparable specific SFR (sSFR) and quenched fractions to field galaxies (Lee et al. 2015; Jian et al. 2020). Moreover, the local SFR–density relation seems to reverse at high redshifts. This implies that there was an epoch in which there was no difference in the SFR between the field and cluster galaxies (Elbaz et al. 2007; Cooper et al. 2008; Hwang et al. 2019). This "transition epoch," when derived from the instantaneous SFR or quenching efficiency through either observations or simulations, seems to converge at $z \sim 1$ (Alberts et al. 2013; Brodwin et al. 2013; Hwang et al. 2019; Pintos-Castro et al. 2019; Williams et al. 2022). On the other hand, considering that there have been many studies indicating various quenching timescales and processes depending on a galaxy's internal properties and environments, it would be mysterious if the transition epoch is universal. Therefore, it is crucial for our understanding of galaxy formation and evolution to pin down such epochs and identify their driving mechanisms.

Numerical simulations have emerged as effective tools for studying the history of galaxy evolution. Since the advent of large-scale $N$-body simulations (Springel et al. 2005), cosmological simulations have become dramatically more sophisticated: to name only a few, they include Horizon-AGN (Dubois et al. 2014), Illustris (Vogelsberger et al. 2014), EAGLE (Crain et al. 2015; Schaye et al. 2015), Mufasa (Davé et al. 2017), IllustrisTNG (Pillepich et al. 2018), SIMBA (Davé et al. 2019), and New-Horizon (Dubois et al. 2021). Along with the advances in our understanding of baryonic physics, these simulations have succeeded in reproducing some key properties of galaxies.

We use Horizon-AGN to investigate the histories of quenching of star formation and assess the level of the reproduction of observed galaxy properties using the simulation. We analyze the quenched states and SFHs of simulated galaxies in various host halo environments and attempt to assess the significance of the internal and external quenching processes on the SFHs of galaxies. In addition, we determine whether there is an epoch where the star formation rates of cluster and field galaxies were equal.

## 2. Methodology

### 2.1. Numerical Simulation

We use the large-scale cosmological hydrodynamic simulation, Horizon-AGN (Dubois et al. 2014), which was performed using the adaptive mesh refinement code, RAMSES (Teyssier 2002). Horizon-AGN uses WMAP7 values to set the cosmological parameters and includes subgrid astrophysics such as gas cooling due to primordial and metallic species and heating by the background UV radiation, star formation, and stellar and AGN feedback (Dubois et al. 2014). The simulation volume is a cube of $100h^{-1}$ Mpc on a side in comoving scale and contains $1024^3$ dark matter particles. The best spatial resolution is $\approx$1 kpc (physical) and the mass resolutions of the dark matter and stellar particles are $8 \times 10^7\,M_\odot$ and $2 \times 10^6\,M_\odot$, respectively. For a more detailed description of Horizon-AGN, refer to Dubois et al. (2014). It has been demonstrated by Kaviraj et al. (2017) that Horizon-AGN shows reasonable agreement with key observational data such as mass function and cosmic star formation history, which are crucial in this study.

### 2.2. Sample Selection

The galaxies and halos in Horizon-AGN are identified using HALOMAKER which is built based on the AdaptaHOP algorithm (Aubert et al. 2004; Tweed et al. 2009). In total, 124,744 galaxies are identified in the last snapshot ($z = 0.018$), and the stellar mass range is $10^{8.2-12.7}M_\odot$. We use the galaxies with a stellar mass greater than $10^{9.5}\,M_\odot$ in the last snapshot to secure the minimum number of stellar particles (900) for reasonable kinematic stability (see Klypin et al. 1999, for the issue of particle evaporation). This criterion leaves 53,226 galaxies as our final sample.

We classify the identified host dark matter halos with a final halo (virial) mass $M_{\rm halo} \geqslant 10^{13}\,M_\odot$ into "group/cluster" halos, as a conventional way (Dariush et al. 2010; Serra & Diaferio 2013; Donnari et al. 2021b). We define the virial radius, $R_{\rm vir}$, as the radius within which the mean density is 200 times the critical density. Note that the term "halo" refers to the main (group/cluster) dark matter halo that hosts multiple satellite galaxies in this study. Using these mass criteria, 428 group/cluster halos were identified. Subsequently, we define their member galaxies using the energy criterion introduced by Han et al. (2018), i.e., by finding galaxies with negative orbital energy within 2.5 times the virial radius. After this cut, we obtain 8228 group/cluster galaxies. These member galaxies in the groups/clusters are our main focus, while the remaining galaxies are used as the control sample. Among the rest, we exclude 3797 galaxies that are within $3R_{\rm vir}$ but not bound to any group/cluster halo from our analysis because we want to highlight the difference between the field and group/cluster galaxies. The remaining 41,201 galaxies are labeled as field galaxies. Figure 1 shows the phase-space distribution of the member galaxies in the Horizon-AGN group/cluster halos at $z = 0.018$. The black line shows the relative velocity ($v$) threshold according to the clustocentric distance ($r$) following Han et al. (2018):

$$\frac{v^2}{2} + \Phi(r) < \Phi(2.5R_{\rm vir}), \tag{1}$$

where $\Phi$ is the gravitational potential of the group/cluster halo calculated from the radial density profile (i.e., the

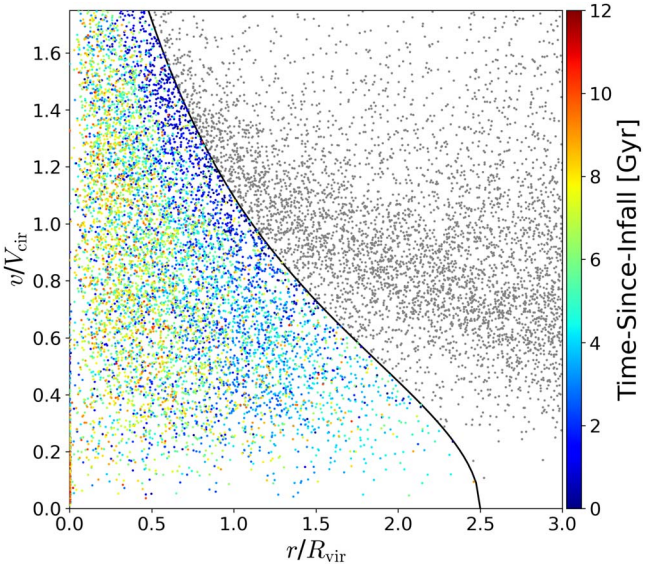


**Figure 1.** Phase-space diagram of Horizon-AGN group/cluster member candidates in the last snapshot ($z = 0.018$). The horizontal axis is the distance of the galaxy from the center of the host halo normalized by the virial radius of the halo. The vertical axis is the relative velocity of the galaxy normalized by the circular velocity. The black line indicates the relative velocity threshold of Han et al. (2018) for selecting satellites. Gray points are galaxies not identified as members, and other color scales show the time since infall of member galaxies (Section 2.2).

Navarro–Frenk–White (NFW) profile):[5]

$$\Phi(s) = \begin{cases} -V_{\rm cir}^2[h(c)g(c)\left(\frac{\ln(1+cs)}{s} - \ln(1+c)\right) \\ -\frac{1}{2}(1-s^2)(h(c)-1)+1], & s < 1 \\ -V_{\rm cir}^2/s, & s \geqslant 1 \end{cases} \quad (2)$$

where $s$ is the clustocentric distance of each galaxy in units of $R_{\rm vir}$ of the host halo ($r/R_{\rm vir}$), $V_{\rm cir}$ is the circular velocity at $R_{\rm vir}$ of the halo ($\sqrt{GM_{\rm vir}R_{\rm vir}}$), and $c$ is the concentration index of the halo assuming the NFW profile. Other terms are defined as follows:

$$h(c) = \left[1 - \frac{c^2 g(c)}{3(1+c)^2}\right]^{-1} \quad (3)$$

$$g(c) = \left[\ln(1+c) - \frac{c}{1+c}\right]^{-1} \quad (4)$$

Figure 1 shows the galaxies within $3R_{\rm vir}$ of our sample group/cluster halos. The member galaxies are color-coded by "time since infall (TSI)." Inspired by previous studies (Oman et al. 2013; Wetzel et al. 2013; Rhee et al. 2017, 2020), we define TSI by measuring the time since the galaxy satisfied the aforementioned membership criterion, Equation (1), in massive halos ($M_{\rm halo} > 10^{13}\,M_\odot$) for the first time. While there are 787 snapshots in Horizon-AGN with intervals of ∼17 Myr, dark matter and gas data are saved only in 61 snapshots with time intervals of ∼250 Myr (see also Khim et al. 2020). As we use the dark matter snapshots to measure the TSI, it is therefore determined with a time resolution of ∼250 Myr. The other galaxies are shown in gray. Member galaxies appear roughly separated in phase space by TSI, which is consistent with the results of Rhee et al. (2017). We can see that this criterion saves the galaxies that are temporarily located outside $R_{\rm vir}$, although they are bound ("back-splashed galaxies"; Gill et al. 2005).

[5] Note that the second condition in this equation was omitted in the original manuscript of Han et al. (2018).

## 3. Results

### 3.1. Quenched Fraction

The fraction in which star formation is quenched is observationally well constrained at least at low redshifts. For example, it is known to depend strongly on the stellar mass and environment of galaxies (e.g., Baldry et al. 2006; Peng et al. 2010; Wetzel et al. 2013). Massive galaxies seem to be more quenched regardless of their environment, whereas low-mass galaxies are more quenched in regions of higher density (Baldry et al. 2006). Such a consensus on the quenched fractions in observations can be used to test the reliability of numerical simulations. In this section, we measure the quenched fractions of our sample of Horizon-AGN galaxies and attempt to understand the impact of stellar and host halo masses on the quenched fraction.

Various methods have been used to measure quenched fractions: double Gaussian fitting on color–magnitude distributions (Baldry et al. 2004; Balogh et al. 2004), color–color (e.g., *UVJ*) distributions (Labbé et al. 2005; Wuyts et al. 2007; Williams et al. 2009), sSFR (Kauffmann et al. 2004; Santini et al. 2009), and distance to the star-forming main sequence (Tacchella et al. 2016; Fang et al. 2018; Pillepich et al. 2019). Donnari et al. (2021a) have reported that the quenched fraction as a function of stellar mass varies significantly with different measurement choices. Bearing such uncertainties in mind, we use sSFR to define quenched galaxies, that is, when $\mathrm{sSFR} < 1/6t_{\rm H}(z)$, where $t_{\rm H}(z)$ is the age of the universe at the epoch of the target redshift ($z$), corresponding to $\sim 10^{-11}$ yr$^{-1}$ at the present epoch (Tacchella et al. 2019).

Figure 2 shows the distribution of the quenched fraction for different stellar and host halo masses. The galaxies are divided into 12 stellar mass bins each of size 0.25 dex, and group/cluster galaxies are additionally divided into eight halo mass bins of size 0.25 dex as well. The number distributions of the group/cluster halos and member galaxies are shown in the top and right panels respectively, with the quenched fractions of field galaxies shown in the left inset. Field galaxies, which are hardly affected by environmental effects, show a gradually increasing quenched fraction with increasing stellar mass. This is often known as the "mass quenching," i.e., more massive galaxies exhibit a higher quenched fraction. A relatively early and short SFH, perhaps associated with feedback effects, is often considered an important process behind mass quenching. Furthermore, we notice three features of the group/cluster galaxies. First, the most massive members ($M_* > 10^{11.5}\,M_\odot$) are virtually all quenched regardless of the host halo mass. This is similar to what has been found for field galaxies and consistent with observations (Peng et al. 2010; Wang et al. 2017, 2018). Hence, it seems that the most massive galaxies are mass-quenched whether they are in the field or in a cluster. We write the fraction of central galaxies in each bin in white letters. The most massive bins are dominated by central galaxies. But whether including or excluding centrals makes little difference to the trend. Second, the satellite galaxies in the most massive halos ($M_{\rm halo} > 10^{14.5}\,M_\odot$) are also predominantly quenched, regardless of the galaxy stellar mass. This implies that

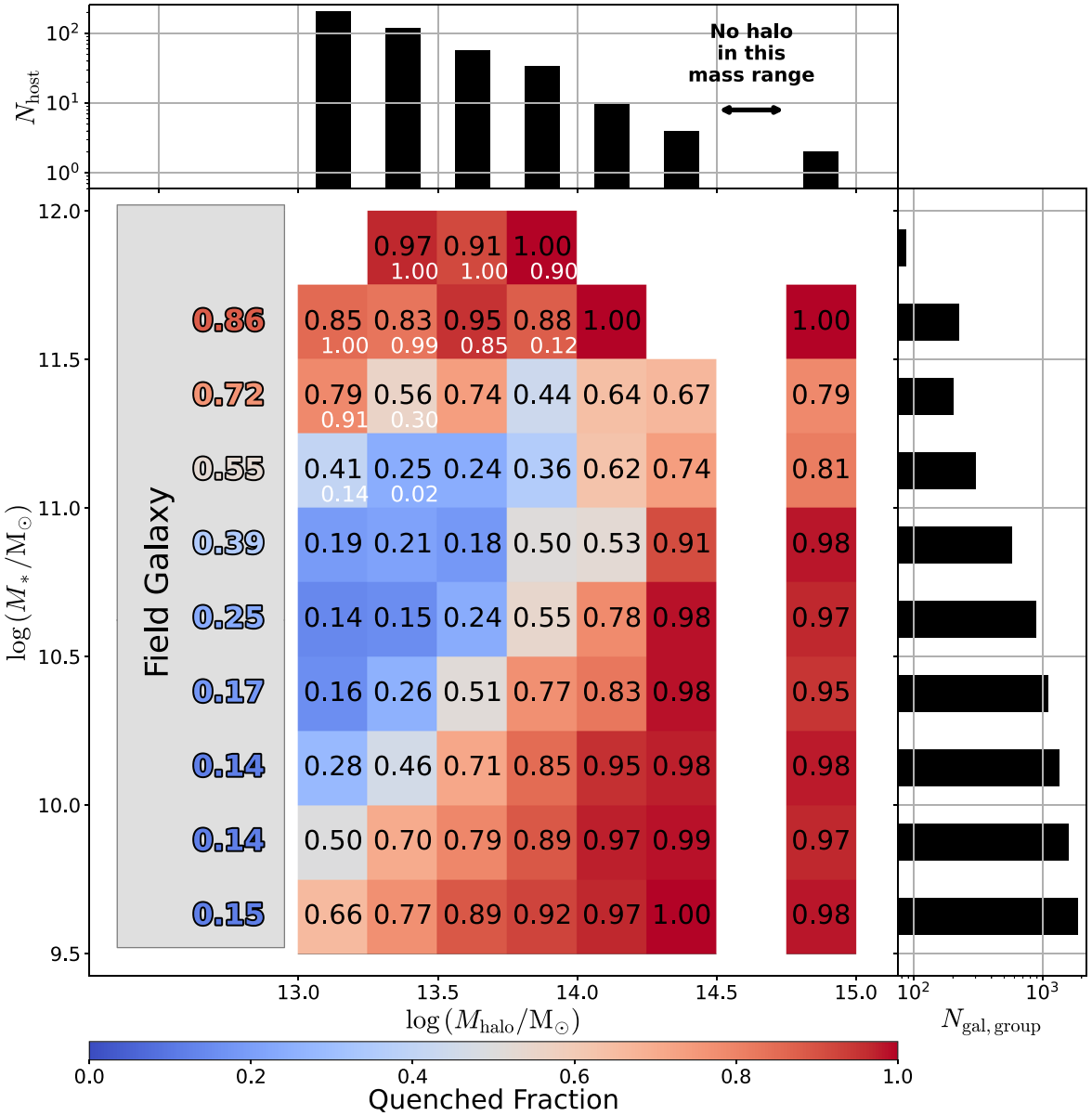


**Figure 2.** Distribution of the quenched fraction of the Horizon-AGN galaxies. The horizontal axis is the host halo mass, and the vertical axis is the stellar mass of member galaxies. The black numbers are quenched fractions color-coded following the key at the bottom and the white numbers are central galaxy fractions. The mean values of the quenched fractions of field galaxies are shown in the gray inset. The top and right panels show the number distributions of the host halos and their member galaxies, respectively. Note that there are only two halos (clusters) of mass $M_{\rm halo} \geqslant 10^{14.5}\,M_\odot$ because of the limited volume of Horizon-AGN (140 Mpc on a side).

environmental effects dominate the quenching process in massive clusters. Lastly, there is a diagonally increasing trend in the quenched fraction (from top left to bottom right in the galaxy mass range of $M_* < 10^{11}\,M_\odot$). The quenched fraction is higher in a more massive halo and in a less massive galaxy. This combined trend is largely consistent with various observations (e.g., Baldry et al. 2006; Peng et al. 2010) as well as with the theoretical expectation based on the ram pressure stripping mechanism (Jung et al. 2018).

The high quenched fraction in low-mass satellite galaxies may call for attention. The nonmonotonic trend of the quenched fraction with respect to the stellar mass is a natural feature of the diagonal trend combined with the mass quenching. However, the observational view of this issue is still unclear. For example, Peng et al. (2010, see their Figure 6) reported that intermediate-mass galaxies in dense environments exhibit smaller fractions of red galaxies than those in the surrounding mass bins, which appears to be consistent with our findings in the Horizon-AGN galaxies. However, Baldry et al. (2006) did not find such a nonmonotonic mass trend, despite being based on similar data. If the Horizon-AGN galaxies are deemed unrealistic owing to the high values of quenched fractions in the low-mass regime, this could be related to the so-called satellite overquenching problem. Kimm et al. (2009) reported that low-mass satellite galaxies exhibit substantially higher quenched fractions than their observational counterparts in several semianalytic models. Moreover, some hydrodynamical simulations report a similar issue, perhaps due to resolution effects. For example, Dickey et al. (2021) investigated resolution effects using the SIMBA and EAGLE simulations, and found that the choice of resolution causes significant differences in the star formation properties of

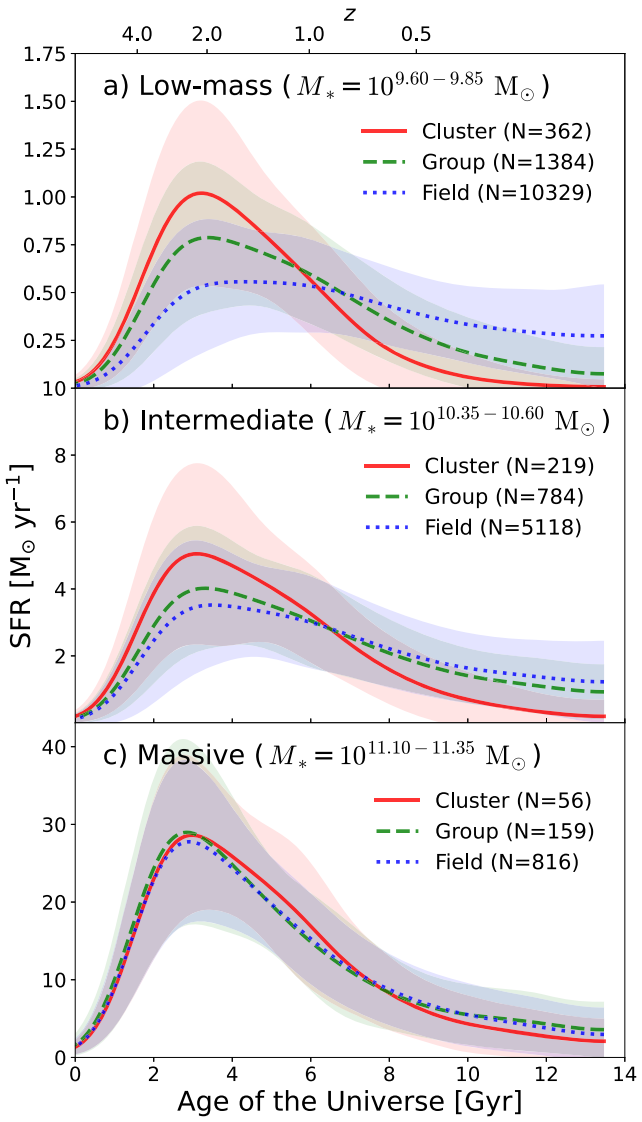


**Figure 3.** Mean SFHs of the Horizon-AGN galaxies of different masses. Other mass bins not shown here are presented in Appendix A. Different colors and line styles represent the different classifications of environments, and the number of galaxies for each subsample is indicated in brackets. The group galaxies (green) mean the galaxies in the host halos of mass $10^{13-14}$ $M_\odot$ and the cluster galaxies (red) are in the halos more massive than $10^{14}$ $M_\odot$. The shaded area shows the $1\sigma$ standard deviation. All the lines are smoothed using a Savitzky–Golay filter and a Gaussian kernel.

low-mass galaxies. Interestingly, Donnari et al. (2021a, 2021b) identified a larger variation in rather more massive galaxies from resolution tests in the TNG simulation.

In summary, Horizon-AGN reproduces the two most robust observational facts: mass quenching at the high-mass end regardless of the environment and severe environmental quenching in massive clusters regardless of galaxy stellar mass. The diagonally increasing trend in the quenched fraction from massive galaxies in low-mass halos to low-mass galaxies in massive halos can be attributed to the phenomenon of ram pressure stripping; however, determining whether it is consistent with observations requires further investigation.

### 3.2. Star Formation History

We have demonstrated that Horizon-AGN reproduces the observed quenched fractions of galaxies well at a given snapshot. Now we focus on the entire SFHs of galaxies and their relationship with stellar mass and host halo mass. There are two conventional methods for building the SFH of a simulated galaxy. One is to track the SFH of the main progenitors in the merger tree (Iyer & Gawiser 2017; Pandya et al. 2017; Zheng et al. 2022). An advantage of this method is that it helps to directly compare with observations at various redshifts because progenitors are observationally identifiable at various redshifts. Another method is to build the SFH based on the age distribution of stellar particles that belong to the galaxy at the last snapshot (Sparre et al. 2015; Diemer et al. 2017; Joshi et al. 2021). This allows for the fact that stars formed in situ may leave the host galaxy while those formed ex situ may join the galaxy later. The approach using the age distribution of stellar particles therefore encodes more complete information about the SFH and the current composition of the galaxy, therefore we use this approach.

Figure 3 shows the SFHs of the Horizon-AGN galaxies in different mass ranges. The top panel shows the case of low-mass galaxies: the shapes of their SFHs are substantially different from each other due to their environments. Cluster galaxies (the red line) are more star-forming at the beginning but quickly quenched. On the other hand, field galaxies (the blue line) exhibit more extended star formation over time. The bottom panel shows the case of massive galaxies, where there is little difference between group/cluster and field galaxies. These results are consistent with previous observational studies (Thomas et al. 2005; Ellison et al. 2018), and moreover, the differences in SFRs near the last snapshot also agree with the results for the quenched fraction (Figure 2). The mass ranges that are missing in Figure 3 show a continuous trend among the presented mass bins (see Appendix A). Thus, the environment significantly affects the SFH of low-mass galaxies. When the SFR is measured at a certain epoch (e.g., the present epoch), it is not likely a transient feature but a result of the whole SFH containing the mass quenching prior to the infall into the host cluster and the environmental quenching after the infall. When the mean properties are compared, cluster galaxies have been more passive than field galaxies for a substantial period (see the top panel of Figure 3). We call the point at which they cross the "transition epoch" and attempt to quantify it in the following sections.

### 3.3. e-*folding Timescale*

The SFH of a galaxy may fluctuate with different timescales due to various physical processes. However, environmental quenching, which is our focus, is rather a long-term process. Thus, we aim to derive simple parameterized functions over time that fit the overall shape of the SFH. We select the "delayed tau-model" (see Wetzel et al. 2013; Rhee et al. 2020, for reference) in this study because it is intuitively consistent with the expectation from simple closed-box systems (e.g., Schmidt 1959) yet versatile enough to allow a delay in the onset of star formation. The following equation is used:

$$\psi(t) = \begin{cases} A(t - T_0)\exp\left(-\frac{t-T_0}{\tau}\right) & t > T_0 \\ 0 & \text{otherwise,} \end{cases} \quad (5)$$

where $\psi$ is the SFR, $t$ is the age of the universe, $A$ is the amplitude, and $T_0$ is the delay in SFH. We consider the $e$-folding timescale $\tau$ a proxy of the quenching timescale. Figure 4 shows the schematic trends for various values of $\tau$

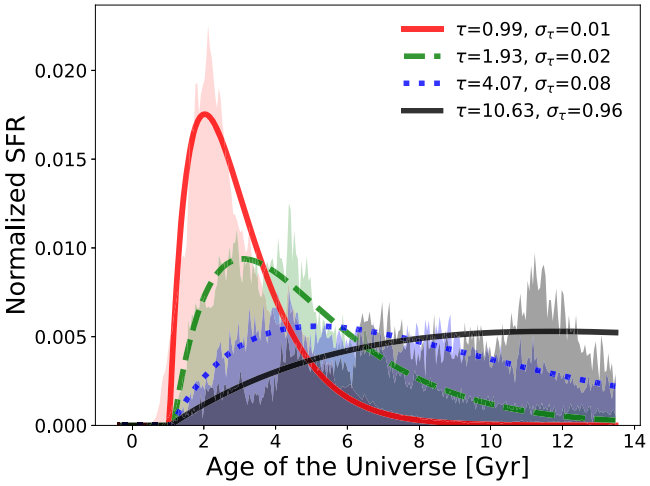


**Figure 4.** SFHs (the shaded area) of four sample Horizon-AGN galaxies and fits using Equation (5) (the lines). The different colors and line styles represent the cases of $\tau \sim 1$, 2, 4, and 10.6 Gyr, respectively. Each line and shaded area are normalized to the integrated SFR for clarity.

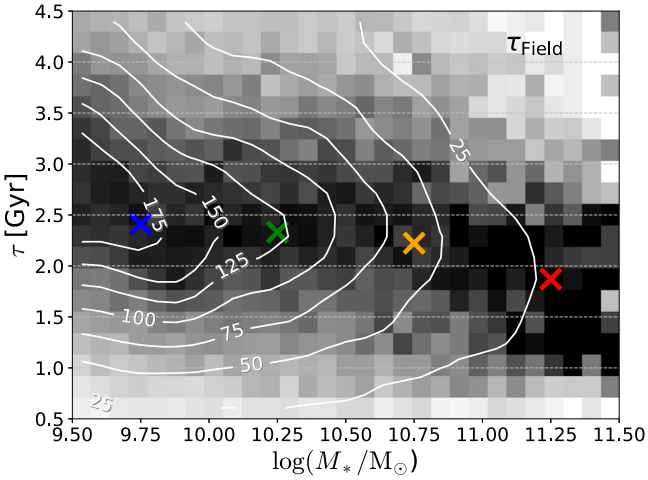


**Figure 5.** Distribution of the $e$-folding timescales ($\tau$) of field galaxies in the Horizon-AGN simulation. The grayscale histogram shows the column-normalized number density, and the white contours show the number of galaxies with labels marked. The median values are presented for four mass bins.

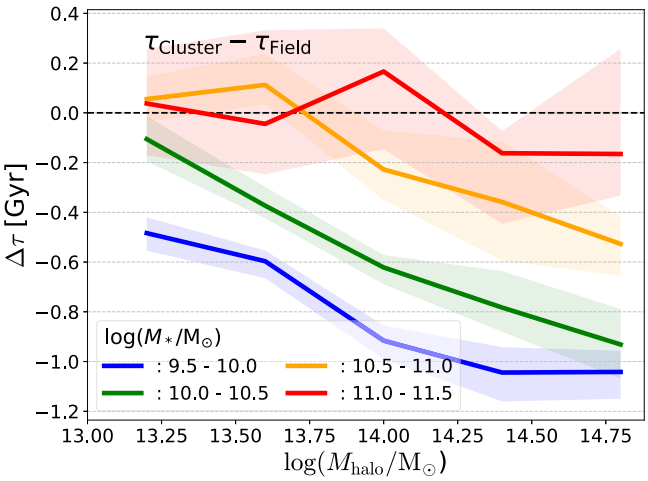


**Figure 6.** Residual values of $\tau$ (cluster galaxies – field galaxies) for different host mass bins, color-coded according to stellar mass bins in the same manner as illustrated in Figure 5. The median value with its standard error of each bin is shown as a shaded line. A small absolute value of $\Delta\tau$ indicates that the environmental effect on the SFH is negligible, while a negative value indicates the existence of the suppression of star formation by environmental effects.

compared to a subsample of simulated galaxies. The $e$-folding timescale, $\tau$, governs the overall shape of the SFH of a galaxy. Moreover, as a larger $\tau$ represents more extended star formation, we can use this model to also fit galaxies with a rising SFR (see the black line in Figure 4).

Now we present how $\tau$ of each galaxy depends on its stellar mass and the environment, as expected in Figure 3. Figure 5 exhibits the values of the field galaxies in the Horizon-AGN simulation. The white contours indicate number density, and the background grayscaled histogram is the column-normalized number density of field galaxies in each bin. The median values are color-coded for each stellar mass bin. The $e$-folding timescales for the Horizon-AGN field galaxies range from 2.7 to 1.7, which agrees with the toy model results of Peng et al. (2010). There is a mild but systematic trend in which more massive galaxies exhibit smaller values of $\tau$, i.e., there is a rapid decline in SFH. Consequently, more massive galaxies are more likely to be quenched early. This explains the quenched fractions of field galaxies (Figure 2). Note that more than half of massive ($M_* > 10^{11}\,M_\odot$) field galaxies are quenched at $z \sim 0$. Now, we take the field galaxies as a control sample to be compared with group/cluster satellite galaxies.

Figure 6 shows the difference in $\tau$ between the field and cluster galaxies ($\Delta\tau$). A negative value of $\Delta\tau$ indicates that cluster galaxies exhibit smaller values of $\tau$, such that their star formation has experienced a more rapid decline than that of field galaxies for a fixed stellar mass. Most satellite galaxies exhibit negative values of $\Delta\tau$, which means that their SFRs have been further decreased by a massive halo environment. This is particularly true for low-mass satellites ($M_* < 10^{10.5}\,M_\odot$) in more massive groups/clusters, where additional environmental quenching appears to be more significant. Conversely, the most massive member galaxies (red line) exhibit little difference ($\Delta\tau \sim 0$) from their field counterparts. It seems that the most massive galaxies are less impacted by their environment. These results are all consistent with the quenched fractions in Figure 2.

It is clear that both stellar and cluster halo masses affect the quenching timescale. However, not all cluster satellites exhibit an environmental effect if they have lived in a massive halo for only a short period of time. Consequently, we want to check the significance of the time spent by a satellite galaxy in its host halo (group/cluster). Herein, we adopt the TSI introduced in Section 2.2. We separate galaxies into several TSI bins and recalculate $\Delta\tau$. Figure 7 shows the satellite galaxies for three different ranges of TSI: recent, intermediate, and ancient infallers arriving in their host halos between 0 and 2 Gyr ago, 2 and 5 Gyr ago, and 5 Gyr or more ago, respectively. Most importantly, there is a clear trend with TSI. The values of $\Delta\tau$ decrease from recent to ancient infallers, indicating the high significance of environmental effects for ancient infallers as expected. However, it is somewhat unexpected that the environmental effect (significantly negative values of $\Delta\tau$) is clearly visible in low-mass galaxies despite the small values of the TSI (blue line in the left panel). This phenomenon can be explained by the combination of two effects. Lower-mass satellites are more easily affected by their host environment in the first place. In addition, when they arrive in massive halos (e.g., $M_{\rm halo} > 10^{14}\,M_\odot$), they are likely to have experienced preprocessing quenching in smaller halo environments before

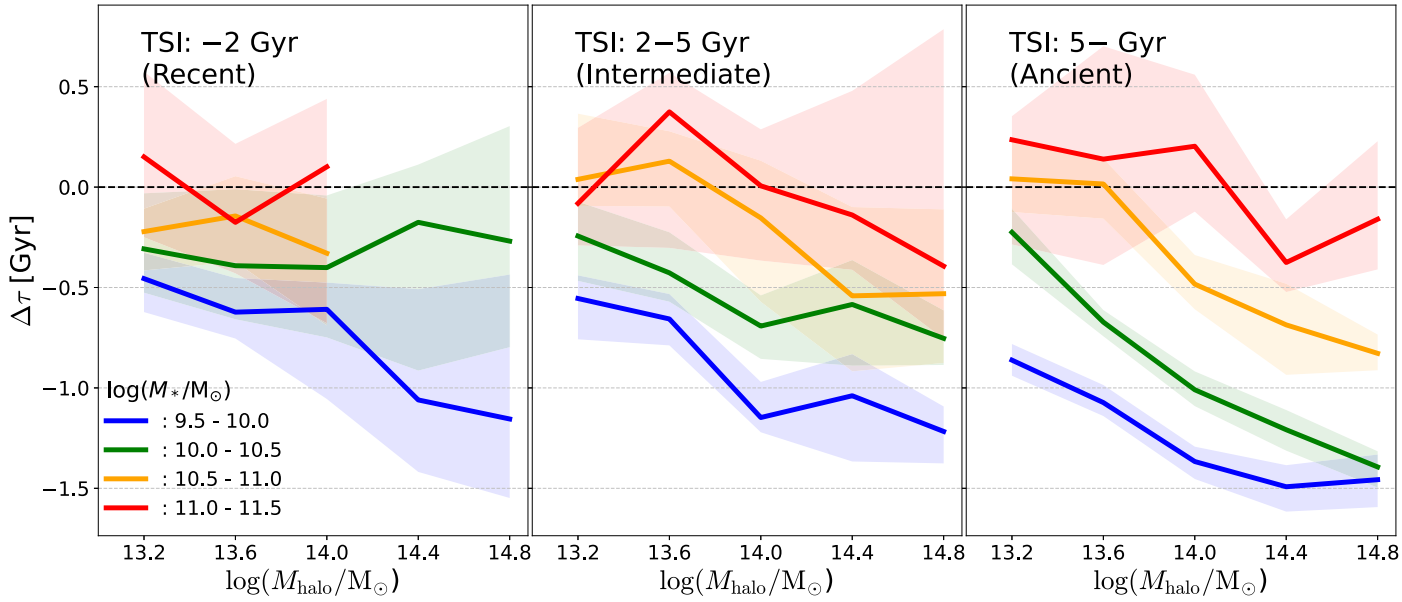


**Figure 7.** The residual values of $\tau$ as a function of the host mass, as in Figure 6 but divided into different TSI bins. From left to right, the TSIs of subsamples have been increased. The color code is similar to the codes shown in Figures 5 and 6 (the red and blue colors denote massive and less massive member galaxies, respectively).

the cluster infall (De Lucia et al. 2012; Han et al. 2018; Jung et al. 2018). Although it may not seem statistically significant, it is interesting to note that the most massive ancient infallers (red line in the right panel) exhibit negative values of $\Delta\tau$, hinting at additional environmental quenching. In our simple analysis of quenched fraction (Section 3.1), and when we ignore the difference in TSI (Figure 6), these massive galaxies seem to remain unaffected by environmental quenching. However, when we delve into the TSI effect, we see a hint of additional environmental effects even in such massive galaxies.

In summary, we have derived the *e*-folding timescales ($\tau$) for the SFH of galaxies in the Horizon-AGN simulation. The *e*-folding timescales exhibit a clear dependence on the galaxy mass and host halo mass. The most massive galaxies seem to have an early and quick SFH almost regardless of the environment. Except for the most massive galaxies (e.g., $M_* > 10^{11}\,M_\odot$), all the satellite galaxies exhibit environmental effects. The magnitude of environmental effects seems larger in lower-mass galaxies and in more massive halos, as expected from the ram pressure stripping process. Moreover, we find that galaxies that have spent more time in their host halo have a shorter *e*-folding timescale, indicating a more significant environmental effect. These findings on the simulated galaxies are largely in agreement with previous observational studies and consistent with basic physical expectations.

## 4. Discussion

### 4.1. Transition Epoch

In the previous section, we established that today's "red and dead" cluster galaxies exhibited higher SFRs at an earlier epoch (Figure 3(a)) and shorter *e*-folding timescales of SFH decay than field galaxies. It is natural that cluster galaxies switched from more active to less active at some point in history, compared with field galaxies (Gerke et al. 2007). We call this moment the "transition epoch." Several studies have suggested similar concepts, that there was an epoch where the relation between SFR and density was reversed (Elbaz et al. 2007; Brodwin et al. 2013; Hwang et al. 2019). While the average SFR of galaxies decreases toward the center of a cluster at low redshifts (Balogh et al. 2000), the trend becomes faint or even reversed at high redshifts. We now attempt to determine whether the Horizon-AGN simulation presents a transition epoch as expected and, if so, whether it is universal or a function of the galaxy stellar mass or group/cluster host halo mass. It is not trivial to uniquely determine the transition epoch in practice, mainly because the actual SFHs of individual simulated galaxies are rather noisy, resulting in multiple crossings between the SFRs of the cluster and field galaxies. We thus use the *cumulative* SFHs to mitigate complications. A full description of the process is provided in Appendix B. In addition, the reliability of an estimated transition epoch depends mainly on how significantly the SFHs of the cluster galaxies are different from those of their field counterparts. Therefore, we perform bootstrapping to estimate the uncertainty in determining the transition epoch.

Figure 8 presents the results in a bubble chart color-coded by the measured transition epochs for each stellar mass and host halo mass bin, in a manner similar to that used for Figure 2. The size of each symbol represents the inverse of the dispersion in the transition epoch measured from bootstrapping; the larger the circle, the more reliable the measurement. The measurements of transition epoch exhibit small values of uncertainty ($<$0.75 Gyr, filled circles with color) in most low-mass galaxies and therefore are reasonably robust. The first notable feature is that transition epochs are reliably measured only for relatively low-mass galaxies of $M_* < 10^{10.5}\ M_\odot$. This is consistent with the results obtained from the *e*-folding timescales (Figure 6). More massive galaxies than that exhibit negligible environmental effects. Next, we notice a diagonal trend from blue to red in the regime of low stellar mass, i.e., as galaxy stellar mass decreases and as host halo mass increases, the transition epoch occurs earlier (larger values in lookback time). This is again consistent with what was learned from the quenched fraction (Figure 2). We present the line for

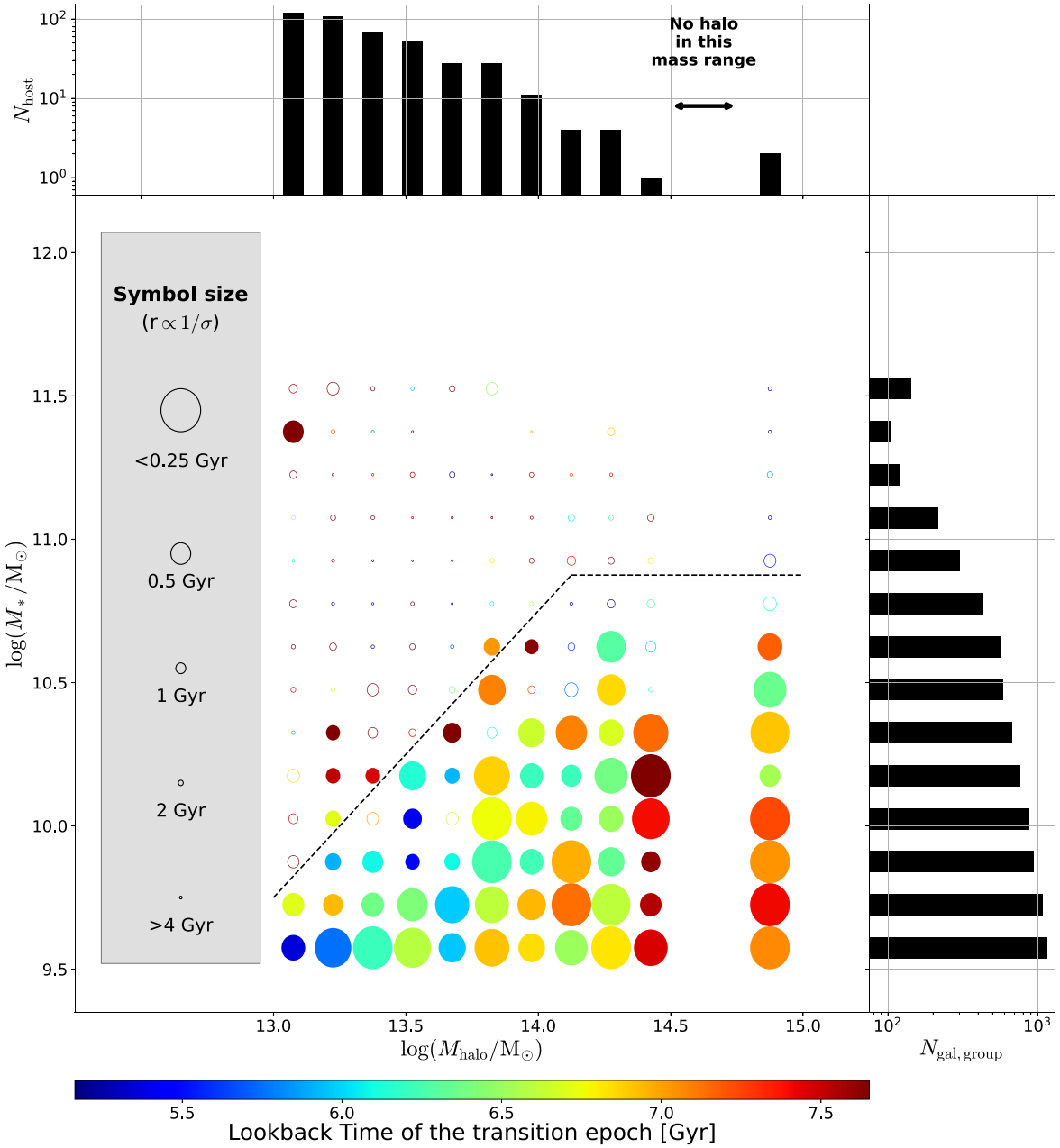


**Figure 8.** Transition epoch for the Horizon-AGN satellite galaxies in a bubble chart. The horizontal axis is the host halo mass, and the vertical axis is the stellar mass of satellite galaxies. The redder color means an earlier transition, and the bluer color means a later transition (color scales at the bottom). We set the size of bubbles based on the distributional uncertainties of transition epochs. Larger symbol size indicates that the transition clearly exists, whereas a small size indicates that there is no transition. The size indicators are shown in the left inset, and we color-coded only bins that exhibited errors smaller than 0.75 Gyr. The black dashed line is a guideline that distinguishes the reliability of the existence of the transition epoch. The top and right panels show numbers of halos and galaxies shown in Figure 2.

$\log(M_{\rm halo}/M_*) = 3.25$ in the figure to guide the eye. It appears that the transition epochs are clearly defined below this line. This will be discussed further in the following section.

The transition epoch ranges from 5.2 to 7.6 Gyr in lookback time depending on the stellar and cluster halo masses. This corresponds to $z \approx 0.56$–$1.02$ according to the standard LCDM cosmology. Considering the age of the universe (≈13.8 Gyr), this range of transition epoch (2.4 Gyr or 17% of the age of the universe) may be viewed as narrow, in which case one may think that there is a "universal" transition epoch. Whether we consider it universal or not, it may clearly be the case in which the most apparent relation between the SFR and environment found in today's galaxies is valid only for half of the cosmic history. It would be interesting to robustly determine the transition epoch in terms of internal and external properties of galaxies in future observations.

### 4.2. Dependence on Halo-to-Stellar Mass Ratio

The main result of our analysis is that the quenched fractions and transition epochs are sensitive to both the stellar mass and host (cluster or group) halo mass: the "diagonal trend." Baldry et al. (2006) expressed the quenched fraction using a *unified formula* that includes the environmental density and stellar mass (see their Equation (10) and Figure 12). Herein, we inspect the quenched fractions and *e*-folding timescales in terms of the halo-to-stellar mass ratio.

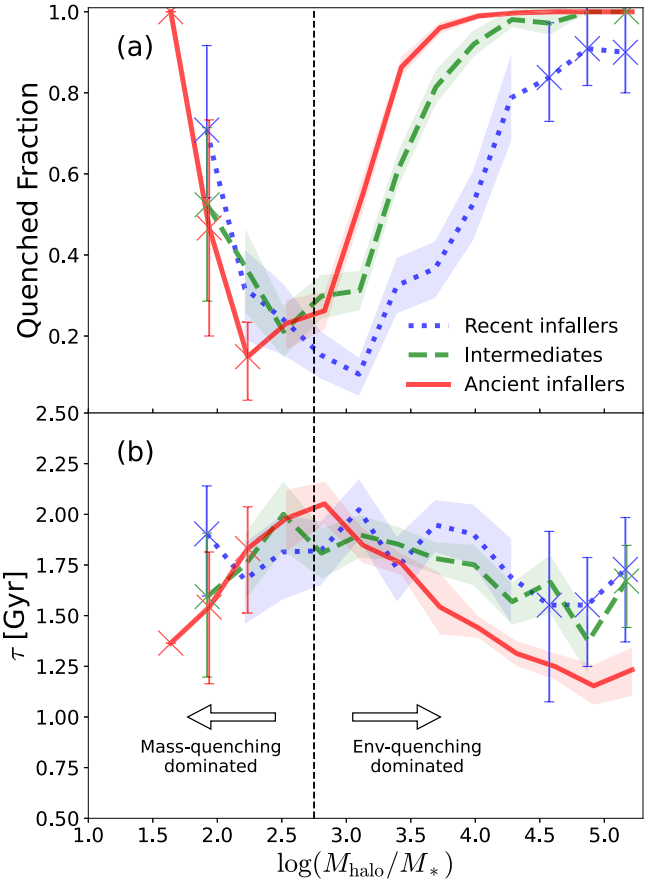


**Figure 9.** a) Quenched fraction of the Horizon-AGN group/cluster galaxies as a function of the halo-to-stellar mass ratio. The red line is the quenched fraction of more ancient infaller galaxies, and the blue line is that of more recent infaller galaxies. The shaded areas show 95% confidence intervals of the estimated quenched fractions. The markers and the error bars are the same as the lines and the shades but have a low number of samples ($N_{\rm gal} \leqslant 50$). The black dashed line at $\log(M_{\rm halo}/M_*) = 2.75$ indicates the arbitrary demarcation where the trend is reversed. (b) The results of $\tau$ as a function of the halo-to-stellar mass ratio for the same galaxies. The color code and detailed format are the same as in (a).

Figure 9(a) shows the quenched fractions of all satellite galaxies as a function of the cluster halo-to-stellar mass ratio. We divide the satellite galaxies into three bins in TSI based on the same criteria used in Figure 7. For galaxies in halos with $\log(M_{\rm halo}/M_*) \gtrsim 2.75$, a clear trend of the quenched fraction increasing with the halo-to-stellar mass ratio exists. This seems to be the main condition for environmental effects to become strong. However, galaxies with low halo-to-stellar mass ratios (i.e., $\log(M_{\rm halo}/M_*) \lesssim 2.75$) exhibit the opposite trend. This is a result of mass quenching. These are mostly massive galaxies in small halos; hence, mass quenching is more effective than environmental quenching. Moreover, ancient infallers in general show higher values of quenched fractions, which illustrates the significance of the TSI effect for the quenched states, as expected.

Similarly, we present the relation between $\tau$ and the mass ratio in Figure 9(b), which is almost a mirror image of Figure 9(a). The environmental effect on the entire SFH of the galaxy is clearly visible at $\log(M_{\rm halo}/M_*) \gtrsim 2.75$. As the halo-to-stellar mass ratio increases, the values of $\tau$ go down to 1 Gyr.

Based on these results, one may want to infer the $e$-folding timescale of SFH decay using the mass ratio and TSI. However, TSI is difficult to determine for observed galaxies in reality (Rhee et al. 2017). Hence, we derive $\tau$ for galaxies in various locations of phase space instead. Figure 10 presents the same information as in Figure 9(b) (i.e., the relation between the mass ratio and $\tau$) but subdivided in different regions of projected position and line-of-sight velocity phase space. To generate this diagram, we randomly generate 300 line-of-sight positions and velocities for each satellite galaxy following the exercise of Rhee et al. (2017) so that the observed data can be easily compared. The phase space of this diagram goes beyond the virialized region marked by the curve in Figure 1. We fit the data (gray dashed lines) using the parameterized formula (black curves):

$$\tau(q) = \alpha \ln(q/2.75) + \beta(q - 2.75) + \tau_* \qquad (6)$$

where $\tau$ is the $e$-folding timescale, $q$ is the logarithm of the mass ratio ($\log(M_{\rm halo}/M_*)$), $\alpha$ is the slope in the low-mass-ratio region, $\beta$ is the slope in the high-mass-ratio region, and $\tau_*$ is the characteristic $e$-folding timescale at $q = 2.75$. We first notice the $n$-shape in the fits of many panels, as shown in Figure 9(b). The relatively more robust satellite members of the group/cluster halos are in the regions inside $r_{\rm proj}/R_{\rm vir} = 1.5$ and $|v_{\rm LOS}|/V_{\rm cir} = 1.5$, i.e., the nine panels marked by the thick black box. Inside this region, the $n$-shape is apparent, and it is more apparent in the satellites close to the phase-space center (i.e., closer to the halo center and with lower values of $|v_{\rm LOS}|/V_{\rm cir}$). The slope of the fit for the high mass ratios ($\beta$) gradually increases from $-1.9$ in the central region of panel (f) to $-1.3$ in the outer region of panel (l). This is all consistent with the results shown in Figure 9(b). In the regions well outside the halos ($R_{\rm vir} > 1.5$, panels (o)–(q)), there are no or few galaxies with mass ratios lower than the pivot value and therefore the fits are monotonic. This is natural because such massive galaxies are likely to be brightest cluster/group galaxies that are rather centrally located in the halo. The fast-moving satellites in panels (a), (b), and (c) are likely recent infallers in group-size halos, which have not been sufficiently affected yet by environmental effects; hence they exhibit larger values of $\beta$ than those of the robust members. The values of $\tau_*$ are remarkably similar among the panels, hinting at a universal demarcation between mass quenching and environmental quenching in the group/cluster galaxies.

## 5. Conclusion

Using the hydrodynamical cosmological simulation, Horizon-AGN, we have investigated how the SFHs of galaxies vary with their internal and external properties. We fit the SFH of each galaxy with a parameterized form and measure the $e$-folding timescale, $\tau$, which quantifies the pace of quenching of star formation. Distinct quenching features have been found in the Horizon-AGN galaxies, and our main results are as follows.

1. Massive galaxies exhibit greater fractions in which star formation is quenched and shorter $e$-folding timescales in their SFHs than low-mass galaxies, regardless of their environments. This implies that the current low star formation rates in massive galaxies are caused by a vigorous star-forming phase and subsequent rapid quenching in the early universe. As expected, mass

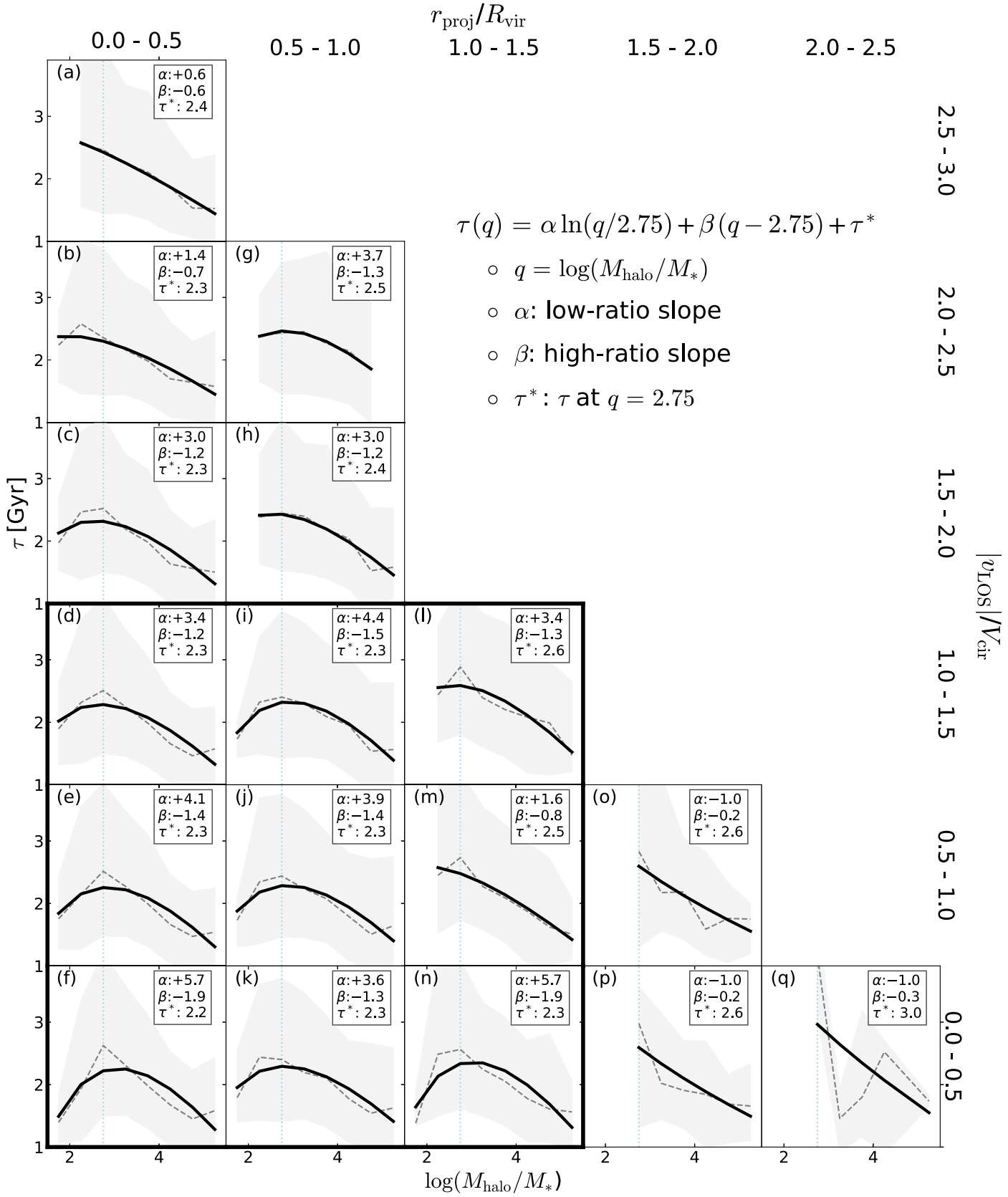


**Figure 10.** *e*-folding timescale as a function of the halo-to-stellar mass ratio. Each panel shows the position on the two-dimensional phase-space diagram. The projected distance ($r_{\rm proj}$) and line-of-sight velocity ($v_{\rm LOS}$) of galaxies are measured from 300 random lines of sight. The gray dashed lines and shades show the median values and their 16th–84th percentile uncertainties, and the black solid lines show the best fits to them. The bins with less than 300 projected galaxies are not displayed. The fitting parameters in Equation (6) are given in each panel. A relatively more robust region of the cluster is roughly marked by the thick box that includes 9 panels.

quenching, which is a dominant process for massive galaxies, is clearly seen in the Horizon-AGN galaxies.

2. Massive cluster environments additionally suppress the star formation of their member galaxies. The galaxies in the most massive cluster halos exhibit significantly higher quenched fractions and substantial drops of $\tau$ compared with their field counterparts. This environmental quenching becomes stronger in more massive halos.
3. The overall star formation activities, including the quenched fraction and the drop of $\tau$, exhibit a diagonal trend in the plane of stellar mass versus halo mass. The additional quenching of satellite galaxies fades when the host halo is not sufficiently massive enough to suppress the star formation of its satellites, which is consistent with theoretical expectations related to ram pressure stripping.
4. Time since infall, i.e., the total time during which a satellite galaxy resides in a group/cluster halo, has a significant impact. The longer a satellite galaxy resides in a group/cluster halo, the more it is affected by environmental quenching. Ancient infallers with larger TSI values exhibit smaller values of $\tau$ than recent infallers. Even the most massive satellites, whose SFH appears to be predominantly determined by mass quenching, show a moderate drop of $\tau$ when they have spent a long time in massive halos.
5. In Horizon-AGN, the transition epoch, where cluster galaxies become less star-forming than field galaxies, occurs 5.2–7.6 Gyr ago in lookback time. This is largely consistent with the previous results of the "reversal epoch," in which SFR–density relations are reversed (Elbaz et al. 2007; Hwang et al. 2019). However, the transition epoch can only be found for low-mass satellites, because massive galaxies do not show much dependence on the environment. It shows a diagonal trend on the plane of stellar mass versus halo mass (low-mass satellites in massive clusters exhibit an early transition epoch), which is consistent with the trend in the $e$-folding timescale as well.
6. The cluster halo-to-stellar mass ratio and TSI may be key parameters for inferring the SFHs of satellite galaxies. Satellite galaxies with different quenching processes are well separated by the mass ratio. With an increase in the mass ratio, the quenched fractions gradually approach unity, and $\tau$ decreases to 1 Gyr. This trend is reversed at $\log(M_{\rm halo}/M_*) \lesssim 2.75$ because, in that domain, mass quenching is more important than environmental quenching. We detect a systematic variation in the relation between $\tau$ and the mass ratio of the satellite galaxies in the observable phase space.

Through this investigation, we have attempted to understand the origin of the star formation properties of galaxies with respect to stellar mass and environment. Horizon-AGN galaxies reproduce the most fundamental features such as mass quenching and environmental quenching. Mass quenching is probably a result of stellar and AGN feedback. A more massive galaxy forms stars more efficiently and consumes cold gas in the early part of cosmic history. The mass of the central black hole scales with the dynamical mass of the galaxy, and thus, the feedback energy from the black hole must play a gradually more important role with increasing stellar mass (Volonteri et al. 2016). The pattern of environmental quenching seems consistent with the expectation from the ram pressure stripping mechanism. As a result of collaboration or competition between the two quenching mechanisms, galaxies do develop and exhibit different properties at different epochs to the extent that some of the most apparent relations are reversed. We are encouraged by the level of detail of the models that reproduce some key properties of present-day galaxies and provide predictions for the high-redshift universe.

We thank the referee for constructive criticism that clarified a few important issues in the original manuscript. S.K.Y. acknowledges the support from the Korean National Research Foundation (2020R1A2C3003769). A.C. acknowledges the support from the Korean National Research Foundation (2022R1A2C100298211). T.K. was supported by the National Research Foundation of Korea (2020R1C1C1007079). R.A.J. was supported by the Yonsei University Research Fund (Yonsei Frontier Lab, Young Researcher Supporting Program) of 2021. This study was partially supported by the Spin(e) grant ANR-13-BS05-0005 of the French Agence Nationale de la Recherche and the Center for Galaxy Evolution Research (2022R1A6A1A03053472). It also relied on the HPC resources of the Horizon Cluster hosted by the Institut d'Astrophysique de Paris. We warmly thank S. Rouberol for running the cluster on which the simulation was postprocessed.

## Appendix A
## Star Formation Histories of Entire Samples

We exhibited the mean SFH of Horizon-AGN galaxies in Figure 3 for representative stellar mass bins. Here we present the same results for all mass bins in Figure A1.

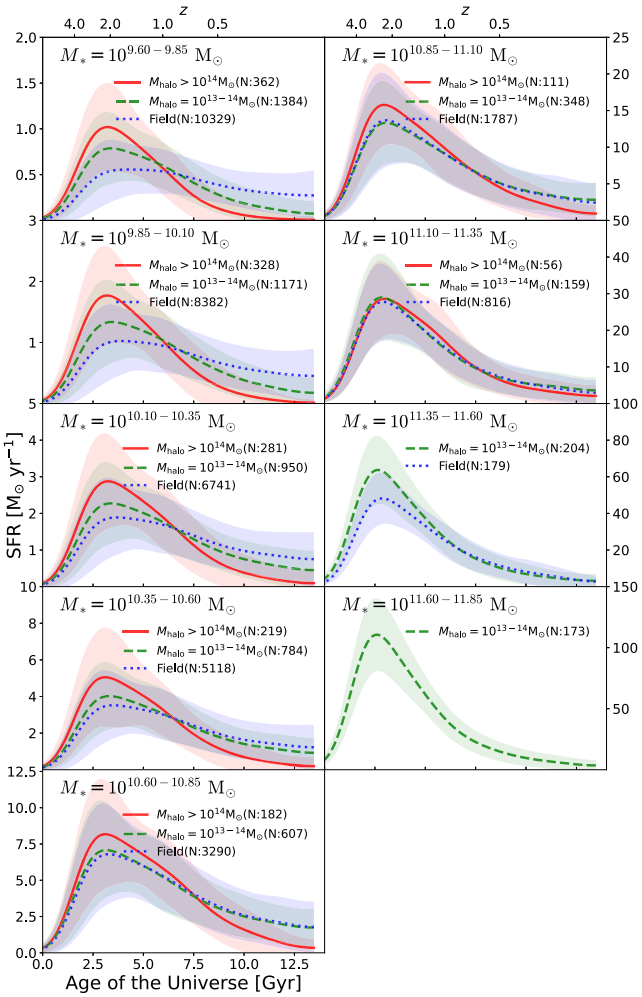


**Figure A1.** Mean SFHs of the Horizon-AGN galaxies of different masses in the same manner as Figure 3.

## Appendix B
## Determination of Transition Epoch

We determine the *transition epoch* as follows. First, we separate our simulated galaxies into stellar mass bins of size 0.25 dex and also separate member galaxies into 0.25 dex bins in host halo mass. We derive the mean SFH of field and cluster galaxies in each bin. A simple solution would then be to determine the intersection point of the SFHs of the field and cluster galaxies. However, as star formation is often bursty and SFHs are very noisy, we decide to use cumulative SFHs. We then calculate the residual cumulative SFH between cluster and field galaxies. We regard the epoch when these residual values reach a maximum as the transition epoch. The procedure is schematically illustrated for models in Figure B1. Furthermore, we can obtain the uncertainty of the estimated transition epoch through bootstrap sampling. Based on 1000 bootstrapped pairs of SFHs, we estimate the mean and its error.

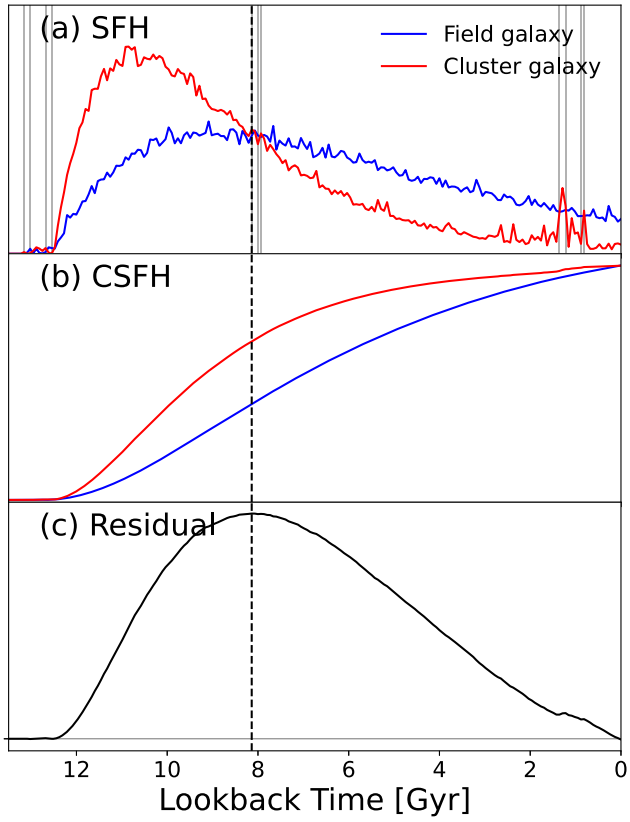


**Figure B1.** Procedure to determine the transition epoch. We generate two mock SFHs with different $\tau$ considering their intrinsic noise. The red and blue lines show the mock SFHs of cluster and field galaxies, respectively. (a) Mean SFH of both samples. (b) Cumulative SFHs. (c) Residuals of the two cumulative SFHs. The gray vertical lines in (a) show all the crossing points that could be misidentified as the transition epoch. The black dashed line shows the determined transition epoch, corresponding to the maximum point of the residual.

## ORCID iDs

Seyoung Jeon https://orcid.org/0000-0002-1270-4465
Sukyoung K. Yi https://orcid.org/0000-0002-4556-2619
Yohan Dubois https://orcid.org/0000-0003-0225-6387
Aeree Chung https://orcid.org/0000-0003-1440-8552
Julien Devriendt https://orcid.org/0000-0002-8140-0422
San Han https://orcid.org/0000-0001-9939-713X
Taysun Kimm https://orcid.org/0000-0002-3950-3997
Christophe Pichon https://orcid.org/0000-0003-0695-6735
Jinsu Rhee https://orcid.org/0000-0002-0184-9589

## References

Alberts, S., Pope, A., Brodwin, M., et al. 2013, MNRAS, 437, 437
Aubert, D., Pichon, C., & Colombi, S. 2004, MNRAS, 352, 376
Baldry, I. K., Balogh, M. L., Bower, R. G., et al. 2006, MNRAS, 373, 469
Baldry, I. K., Glazebrook, K., Brinkmann, J., et al. 2004, ApJ, 600, 681
Balogh, M. L., Baldry, I. K., Nichol, R., et al. 2004, ApJ, 615, L101

Balogh, M. L., Morris, S. L., Yee, H. K. C., Carlberg, R. G., & Ellingson, E. 1999, ApJ, 527, 54
Balogh, M. L., Navarro, J. F., & Morris, S. L. 2000, ApJ, 540, 113
Boselli, A., & Gavazzi, G. 2006, PASP, 118, 517
Brodwin, M., Stanford, S. A., Gonzalez, A. H., et al. 2013, ApJ, 779, 138
Butcher, H., & Oemler, A. J. 1978, ApJ, 226, 559
Chung, A., van Gorkom, J. H., Kenney, J. D. P., & Vollmer, B. 2007, ApJ, 659, L115
Cooper, M. C., Newman, J. A., Weiner, B. J., et al. 2008, MNRAS, 383, 1058
Crain, R. A., Schaye, J., Bower, R. G., et al. 2015, MNRAS, 450, 1937
Croton, D. J., Springel, V., White, S. D., et al. 2006, MNRAS, 365, 11
Dariush, A. A., Raychaudhury, S., Ponman, T. J., et al. 2010, MNRAS, 405, 1873
Davé, R., Anglés-Alcázar, D., Narayanan, D., et al. 2019, MNRAS, 486, 2827
Davé, R., Rafieferantsoa, M. H., Thompson, R. J., & Hopkins, P. F. 2017, MNRAS, 467, 115
De Lucia, G., Weinmann, S., Poggianti, B. M., Aragón-Salamanca, A., & Zaritsky, D. 2012, MNRAS, 423, 1277
Dekel, A., & Silk, J. 1986, ApJ, 303, 39
Dickey, C. M., Starkenburg, T. K., Geha, M., et al. 2021, ApJ, 915, 53
Diemer, B., Sparre, M., Abramson, L. E., & Torrey, P. 2017, ApJ, 839, 26
Donnari, M., Pillepich, A., Nelson, D., et al. 2021a, MNRAS, 506, 4760
Donnari, M., Pillepich, A., Joshi, G. D., et al. 2021b, MNRAS, 500, 4004
Dressler, A. 1980, ApJ, 236, 351
Dubois, Y., Beckmann, R., Bournaud, F., et al. 2021, A&A, 651, A109
Dubois, Y., Pichon, C., Welker, C., et al. 2014, MNRAS, 444, 1453
Elbaz, D., Daddi, E., Le Borgne, D., et al. 2007, A&A, 468, 33
Ellison, S. L., Sánchez, S. F., Ibarra-Medel, H., et al. 2018, MNRAS, 474, 2039
Fabian, A. C. 2012, ARA&A, 50, 455
Fang, J. J., Faber, S. M., Koo, D. C., et al. 2018, ApJ, 858, 100
Gerke, B. F., Newman, J. A., Faber, S. M., et al. 2007, MNRAS, 376, 1425
Gill, S. P., Knebe, A., & Gibson, B. K. 2005, MNRAS, 356, 1327
Gnedin, O. Y. 2003, ApJ, 589, 752
Governato, F., Brook, C., Mayer, L., et al. 2010, Natur, 463, 203
Gunn, J. E., Gott, J., & Richard, I. 1972, ApJ, 176, 1
Han, S., Smith, R., Choi, H., et al. 2018, ApJ, 866, 78
Hogg, D. W., Blanton, M. R., Eisenstein, D. J., et al. 2003, ApJ, 585, L5
Hopkins, P. F., Grudić, M. Y., Wetzel, A., et al. 2020, MNRAS, 491, 3702
Hwang, H. S., Shin, J., & Song, H. 2019, MNRAS, 489, 339
Iyer, K., & Gawiser, E. 2017, ApJ, 838, 127
Iyer, K. G., Tacchella, S., Genel, S., et al. 2020, MNRAS, 498, 430
Jian, H.-Y., Lin, L., Koyama, Y., et al. 2020, ApJ, 894, 125
Joshi, G. D., Pillepich, A., Nelson, D., et al. 2021, MNRAS, 508, 1652
Jung, S. L., Choi, H., Wong, O. I., et al. 2018, ApJ, 865, 156
Kauffmann, G., White, S. D., Heckman, T. M., et al. 2004, MNRAS, 353, 713
Kaviraj, S., Laigle, C., Kimm, T., et al. 2017, MNRAS, 467, 4739
Khim, D. J., Yi, S. K., Dubois, Y., et al. 2020, ApJ, 894, 106
Kimm, T., Somerville, R. S., Yi, S. K., et al. 2009, MNRAS, 394, 1131
Klypin, A., Gottlober, S., Kravtsov, A. V., & Khokhlov, A. M. 1999, ApJ, 516, 530
Labbé, I., Huang, J., Franx, M., et al. 2005, ApJ, 624, L81
Larson, R. B. 1974, MNRAS, 169, 229
Larson, R. B., & Starrfield, S. 1971, A&A, 13, 190
Larson, R. B., Tinsley, B. M., & Caldwell, C. N. 1980, ApJ, 237, 692
Lee, S. K., Im, M., Kim, J. W., et al. 2015, ApJ, 810, 90
Mihos, J. C. 2004, in Clusters of Galaxies: Probes of Cosmological Structure and Galaxy Evolution, ed. J. S. Mulchaey, A. Dressler, & A. Oemler (Cambridge: Cambridge Univ. Press), 277
Moore, B., Katz, N., Lake, G., Dressler, A., & Oemler, A. 1996, Natur, 379, 613
Moore, B., Lake, G., & Katz, N. 1998, ApJ, 495, 139
Oman, K. A., Hudson, M. J., & Behroozi, P. S. 2013, MNRAS, 431, 2307
Pandya, V., Brennan, R., Somerville, R. S., et al. 2017, MNRAS, 472, 2054
Peirani, S., Dubois, Y., Volonteri, M., et al. 2017, MNRAS, 472, 2153
Peng, Y.-J., Lilly, S. J., Kovač, K., et al. 2010, ApJ, 721, 193
Pillepich, A., Nelson, D., Springel, V., et al. 2019, MNRAS, 490, 3196
Pillepich, A., Springel, V., Nelson, D., et al. 2018, MNRAS, 473, 4077
Pintos-Castro, I., Yee, H. K. C., Muzzin, A., Old, L., & Wilson, G. 2019, ApJ, 876, 40
Quilis, V., Moore, B., & Bower, R. 2000, Sci, 288, 1617
Rafferty, D. A., McNamara, B. R., Nulsen, P. E. J., & Wise, M. W. 2006, ApJ, 652, 216
Rhee, J., Smith, R., Choi, H., et al. 2017, ApJ, 843, 128
Rhee, J., Smith, R., Choi, H., et al. 2020, ApJS, 247, 45
Richstone, D. O. 1976, ApJ, 204, 642
Santini, P., Fontana, A., Grazian, A., et al. 2009, A&A, 504, 751
Schaye, J., Crain, R. A., Bower, R. G., et al. 2015, MNRAS, 446, 521
Schmidt, M. 1959, ApJ, 129, 243
Serra, A. L., & Diaferio, A. 2013, ApJ, 768, 116
Sheen, Y.-K., Yi, S. K., Ree, C. H., et al. 2016, ApJ, 827, 32
Smith, R., Choi, H., Lee, J., et al. 2016, ApJ, 833, 109
Smith, R., Sánchez-Janssen, R., Beasley, M. A., et al. 2015, MNRAS, 454, 2502
Sparre, M., Hayward, C. C., Springel, V., et al. 2015, MNRAS, 447, 3548
Springel, V., White, S. D., Jenkins, A., et al. 2005, Natur, 435, 629
Strateva, I., Ivezić, Ž, Knapp, G. R., et al. 2001, AJ, 122, 1861
Tacchella, S., Dekel, A., Carollo, C. M., et al. 2016, MNRAS, 457, 2790
Tacchella, S., Diemer, B., Hernquist, L., et al. 2019, MNRAS, 487, 5416
Teyssier, R. 2002, A&A, 385, 337
Thomas, D., Maraston, C., Bender, R., & de Oliveira, C. M. 2005, ApJ, 621, 673
Tonnesen, S., Bryan, G. L., & van Gorkom, J. H. 2007, ApJ, 671, 1434
Tweed, D., Devriendt, J., Blaizot, J., Colombi, S., & Slyz, A. 2009, A&A, 506, 647
Vogelsberger, M., Genel, S., Springel, V., et al. 2014, MNRAS, 444, 1518
Volonteri, M., Dubois, Y., Pichon, C., & Devriendt, J. 2016, MNRAS, 460, 2979
Wang, E., Wang, H., Mo, H., et al. 2018, ApJ, 860, 102
Wang, H., Mo, H., Chen, S., et al. 2017, ApJ, 852, 31
Wetzel, A. R., Tinker, J. L., Conroy, C., & van den Bosch, F. C. 2013, MNRAS, 432, 336
Whitworth, A. 1979, MNRAS, 186, 59
Williams, C. C., Alberts, S., Spilker, J. S., et al. 2022, ApJ, 929, 35
Williams, R. J., Quadri, R. F., Franx, M., van Dokkum, P., & Labbé, I. 2009, ApJ, 691, 1879
Wuyts, S., Labbe, I., Franx, M., et al. 2007, ApJ, 655, 51
Yi, S. K., Lee, J., Jung, I., Ji, I., & Sheen, Y. K. 2013, A&A, 554, 2
Zheng, Y., Dave, R., Wild, V., & Montero, F. R. 2022, MNRAS, 513, 27